



**HAL**  
open science

# Advective transport caused by intraseasonal Rossby waves: A key player of the high chlorophyll variability off the Peru upwelling region

Céline Bonhomme, Olivier Aumont, Vincent Echevin

► **To cite this version:**

Céline Bonhomme, Olivier Aumont, Vincent Echevin. Advective transport caused by intraseasonal Rossby waves: A key player of the high chlorophyll variability off the Peru upwelling region. *Journal of Geophysical Research*, 2007, 112, pp.09018. 10.1029/2006JC004022 . hal-00770624

**HAL Id: hal-00770624**

**<https://hal.science/hal-00770624>**

Submitted on 29 Oct 2021

**HAL** is a multi-disciplinary open access archive for the deposit and dissemination of scientific research documents, whether they are published or not. The documents may come from teaching and research institutions in France or abroad, or from public or private research centers.

L'archive ouverte pluridisciplinaire **HAL**, est destinée au dépôt et à la diffusion de documents scientifiques de niveau recherche, publiés ou non, émanant des établissements d'enseignement et de recherche français ou étrangers, des laboratoires publics ou privés.

Copyright

## Advective transport caused by intraseasonal Rossby waves: A key player of the high chlorophyll variability off the Peru upwelling region

C. Bonhomme,<sup>1</sup> O. Aumont,<sup>2</sup> and V. Echevin<sup>1</sup>

Received 20 November 2006; revised 2 May 2007; accepted 23 May 2007; published 20 September 2007.

[1] The upwelling region off Peru between 5°S and 12°S is characterized by high offshore intraseasonal variability in sea-surface productivity due to westward propagating chlorophyll anomalies, whose magnitude can reach half the variance of total chlorophyll variations. Spectral analyses of SSH, SST and chlorophyll satellite data show that these events are generated by intraseasonal Rossby waves. The almost constant phase shift between chlorophyll and altimetric signals suggests a physical mechanism dominated by horizontal advection, which is confirmed by the use of a simple conceptual model. Furthermore, an increase from the north to the south in the detected Rossby wave periods, correlated with a decrease in the wavelengths and phase velocities of the wave, suggests the presence of a second baroclinic mode north of 8°S and of a first baroclinic mode south of this latitude. The latitude of this transition is consistent with the theory of critical latitudes, which specifies that at a given latitude, only Rossby wave with periods below a threshold period, depending on the baroclinic structure of the wave, can propagate offshore. According to this theory, second baroclinic mode Rossby waves with periods greater than 130 days are supposed to propagate off the South American coast north of 8°S, the corresponding critical latitude.

**Citation:** Bonhomme, C., O. Aumont, and V. Echevin (2007), Advective transport caused by intraseasonal Rossby waves: A key player of the high chlorophyll variability off the Peru upwelling region, *J. Geophys. Res.*, *112*, C09018, doi:10.1029/2006JC004022.

### 1. Introduction

[2] The Peru region is characterized by a permanent coastal upwelling owing to the southeasterly trade winds oriented parallel to the coast throughout the year. This upwelling regime brings cold, nutrient-rich subsurface waters to the surface, which sustains an intense primary productivity along the coast [Chavez, 1995; Carr, 2002] and makes the Peru-Chile system one of the world's most productive regions in terms of fisheries [Alheit and Bemal, 1993]. The high phytoplankton biomass can extend hundreds of kilometers offshore, whereas the physical boundary of the upwelling, namely the upwelling density front, remains close to the coast (typically less than 100 km). The wider extension of the productive region relative to the physical upwelling is a common feature observed in all eastern boundary upwelling systems [Carr *et al.*, 2002].

[3] The ocean off Peru-Chile is characterized by strong interannual fluctuations in sea-surface chlorophyll concentrations associated with the El Niño–Southern Oscillation, with maxima always located along the coast [Thomas *et al.*, 2001; Carr *et al.*, 2002]. On the other hand, when considering all the timescales, the normalized standard deviation

of sea-surface chlorophyll is maximum at a distance of 100–500 km from the coast, whereas it is significantly smaller just off the coast (Figure 1). Thus, surprisingly, the most productive region is not the place where the relative fluctuations are the strongest. Understanding the processes, either physical or biological, that drive this variability, is the main goal of the present work.

[4] During the last few years, there have been numerous studies on open-ocean planetary waves (or Rossby waves) based on sea color observations. These studies have revealed sea level and chlorophyll anomalies propagating westward at the same speed in all oceanic basins [Cipollini *et al.*, 2001; Killworth *et al.*, 2004]. These westward propagating features have large spatial scales ( $\gg 10^2$  km) and are also distinct from westward propagating eddies, which have smaller spatial scales and higher kinetic energy levels [McGillicuddy *et al.*, 1998; Le Traon, 1991]. Different hypotheses have been proposed to explain how Rossby waves can modify sea-surface chlorophyll concentration. The proposed mechanisms are either based on chlorophyll transport by the Rossby wave associated currents or on transport of nutrients and/or organisms by the currents, which could result in an enhanced primary productivity. First, Rossby waves can act by a purely physical mechanism: meridional currents associated to the waves can transport chlorophyll meridionally in the presence of a meridional gradient of chlorophyll such that chlorophyll anomalies propagate westward with the wave [Killworth *et al.*, 2004]. A second physical mechanism has been called the “rototiller effect” [Siegel, 2001]. The vertical velocity

<sup>1</sup>Laboratoire d’Océanographie et de Climatologie: Experimentation et Approches Numériques IRD/ENPC/IPSL, Paris, France.

<sup>2</sup>Laboratoire d’Océanographie et de Climatologie: Experimentation et Approches Numériques IRD/ENPC/IPSL, Plouzané France.

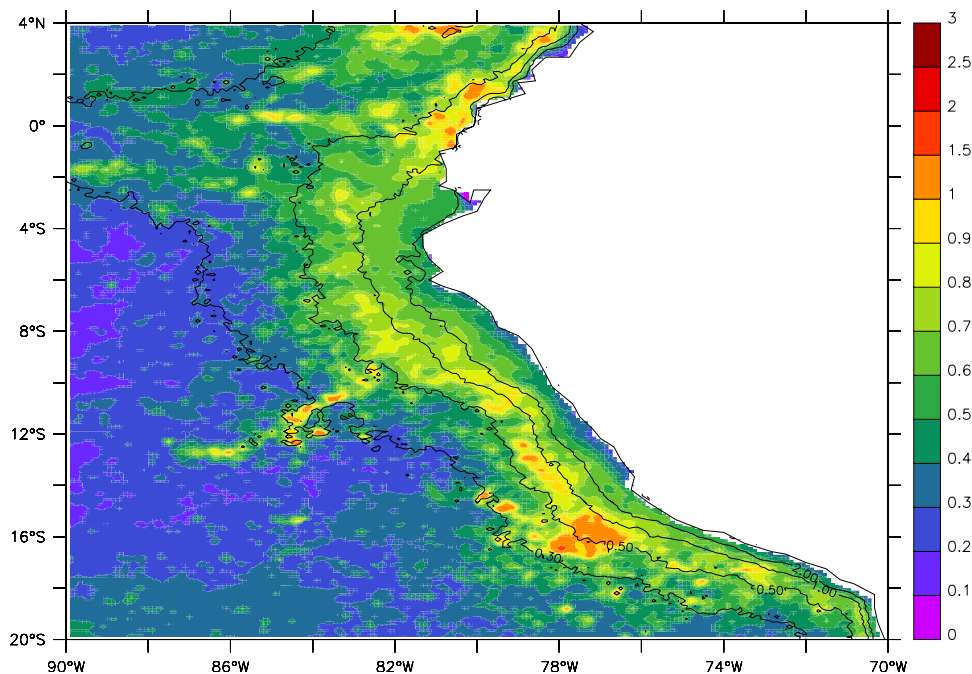


**Figure 1.** Standard deviation of normalized chlorophyll concentration. Normalized chlorophyll is defined as  $Chl / \overline{Chl}$  at each grid point, where the overbar denotes temporal mean. The contours represent 0.3, 0.5, 1 and 2  $\text{mg}/\text{m}^3$  chlorophyll concentration isolines.

associated to the leading edge of the wave can pump subsurface nutrients into the surface layer thus stimulating phytoplankton growth. In that case, there is always a lag between the nutrient injection and the occurrence of the bloom. Furthermore, this upwelling may also raise the deep chlorophyll maximum into the mixed layer [Kawamiya and Oeschies, 2001]. Last, floating particles may accumulate into the convergence zones created by the quasigeostrophic currents associated with the wave. Thus Rossby waves act as a “hay-rake” for chlorophyll-rich floating materials, which can be detected by remote sensing [Dandonneau *et al.*, 2003].

[5] Previous studies have focused on the open ocean, away from coastal areas, which are often affected by high eddy activity that can mask the more organized SSH anomalies generated by Rossby waves. The upwelling region off Peru is particularly interesting as the background sea-surface chlorophyll concentration is higher than in most open ocean regions. Moreover, this low-latitude region is characterized by “boundary-driven” Rossby waves propagation, which is not the case of the middle of subtropical gyres where Rossby waves could be generated locally by the wind stress curl [Fu and Qiu, 2002]. With chlorophyll levels higher than in offshore regions, one can expect stronger chlorophyll gradients and a more evident signature of Rossby waves on the chlorophyll signal than in the middle of the subtropical gyre for instance, which should allow for a more accurate determination of the processes involved. Moreover, the meridional chlorophyll gradient, a crucial ingredient in the hypothesis of Rossby waves-related horizontal advection of chlorophyll, is enhanced because of the strong nearshore productivity and because of the northwest to southeast orientation of the coastline (see Figure 2). We can expect the westward propagating eddy

field created by the Rossby wave will transport chlorophyll from the highly productive region to the open ocean quite efficiently.

[6] The present study aims at characterizing and quantifying the impact of Rossby waves on primary productivity off Peru. The analysis is restricted to the  $5^{\circ}\text{S}$ – $12^{\circ}\text{S}$  latitude band, away from the equatorial region where the high-productivity area extends farthest from the coast. Section 2 describes the satellite data products, the spectral analysis techniques used here, as well as the conceptual model of Killworth *et al.* [2004]. In section 3, the observed chlorophyll and westward propagating SSH features are charac-

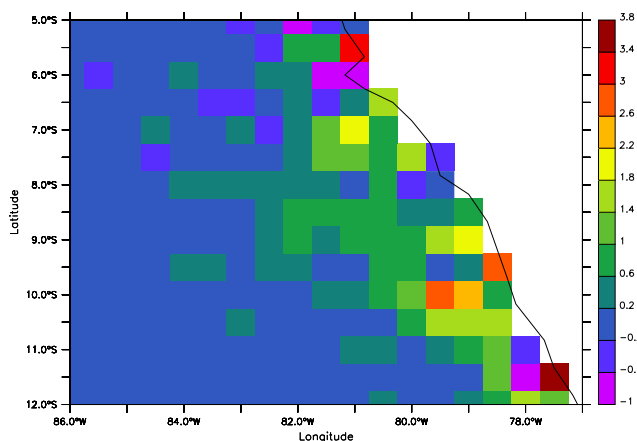


**Figure 2.** Meridional gradient ( $10^5 \text{ mg Chl}/\text{m}^4$ ) of the SeaWiFS 1998–2004 mean chlorophyll concentration. Data are plotted on a  $0.5^{\circ} \times 0.5^{\circ}$  grid to reduce the short-scale noise.

terized and analyzed with the spectral techniques. Additionally, the simple conceptual model is used to investigate the potential physical/biological mechanisms responsible for the signal in surface chlorophyll. In section 4, the results and the uncertainties are discussed, before some conclusions are drawn.

## 2. Material and Method

### 2.1. Data Products

#### 2.1.1. Sea Surface Height (SSH)

[7] The AVISO merged TOPEX-POSEIDON/ERS-1-2 sea level anomalies for the period October 1992 to June 2004 were used. The data product consists of 7-day means of SSH on a  $0.3^\circ \times 0.3^\circ$  spatial grid.

#### 2.1.2. SST

[8] The SST product is the Weekly Global Gridded MultiChannel Sea-Surface Temperature (MCSST) derived from the NOAA AVHRR. These 7-day data are available for the period 11 November 1981 to 7 February 2001. These data have been regridded onto the grid used for the SSH data product ( $0.3^\circ \times 0.3^\circ$ ).

#### 2.1.3. Tide Gauges

[9] Tide gauge data from the Sea Level Center of Hawaii University were used. Among all of the available tide gauge data along the South American coast between  $5^\circ\text{S}$  and  $12^\circ\text{S}$ , only data for two sites (Lobos at  $6^\circ\text{S}$  and Callao at  $12^\circ\text{S}$ ) demonstrated high correlations with TOPEX/POSEIDON data interpolated at the coast, and thus we have opted to include only those two tide gauge time series in this study.

#### 2.1.4. Sea-Surface Chlorophyll

[10] In this study, we have used SeaWiFS global area coverage (GAC) level 3 data from NASA-GSFC DAAC, processed with the version 4 chlorophyll algorithm [O'Reilly *et al.*, 1998]. These data are daily composites of chlorophyll concentration in  $\text{mg Chl/m}^3$ , covering a period of 7 years, from September 1997 to June 2004. We chose to remove data until beginning of June 1999, which corresponds to the termination of a strong La Niña event [Thomas *et al.*, 2001].

### 2.2. Gap-Filling Procedure for Sea-Surface Chlorophyll

[11] As certain periods of the year, mainly austral winter, are particularly cloudy, the chlorophyll signal has been extrapolated by averaging pixels around the missing values simultaneously in space and time. This filling procedure has been applied on the daily product binned on the original  $0.0879^\circ \times 0.0879^\circ$  grid. Chlorophyll values present in a spatiotemporal radius of 8 days and of  $0.0879^\circ$  around the missing values have been averaged, which is relevant for the temporal and spatial scales of chlorophyll variability. When no data were available in this radius of influence, the gap was not filled. After this interpolation procedure, the data were regridded onto the 7-day,  $0.3^\circ \times 0.3^\circ$  SSH grid. This step was necessary to improve the coverage of sea-color data. However, this interpolation technique could not sufficiently improve the data coverage during wintertime, leading us to disregard that period of the year. Only 30 weeks of SeaWiFS data were kept each year from 1999 to 2003. The data analysis described below was performed on each of these truncated years.

### 2.3. Extraction and Filtering of the Westward Propagating Signal

[12] The chlorophyll, SSH and SST signals have been analyzed using time-space 2D-Fourier transforms at each latitude. This 2D-Fourier analysis was performed after all gaps were filled using a nearest neighbor linear interpolation on each truncated sea-surface chlorophyll time series. At each latitude, the signal was decomposed into the angular frequency and wave number components present in the signal. Then a Hanning band-pass filter, passing 30 to 240 days in time and 1 to 10 degrees in space, was applied to remove the high-frequency noise, the seasonal cycle as well as any stationary waves. Additionally, the 2D-Fourier analysis was also used to separate eastward and westward propagating signals. As expected, the westward propagating signal largely dominated the eastward component on chlorophyll, SSH and SST data: The ratio of the westward to eastward peak amplitude was close to 3 for chlorophyll data almost everywhere in the region of study (this ratio was higher for SSH data in which the Rossby wave signal is clearer). Since, in this study, we focus on the intraseasonal Rossby wave, the noise was reduced by keeping only westward propagating features.

### 2.4. Spectral Analysis

[13] Autospectra and cross spectra of SSH and sea-surface chlorophyll were calculated at a spatial resolution of  $1/3^\circ$  between  $5^\circ\text{S}$  and  $12^\circ\text{S}$ .

#### 2.4.1. Autospectra

[14] An autospectral analysis allows for an identification of the most energetic spatial and temporal scales in a given signal. The sea-surface chlorophyll autospectrum was calculated by averaging the four autospectra corresponding to the four selected SeaWiFS years. Each sample spans 30 weeks corresponding to the noncloudy period in the chlorophyll signal. This was necessary in order to obtain a good estimation of the mean autospectrum and to avoid introducing a bias by adding spurious frequencies during the cloudy winter period. As we used interpolated SSH, there were no gaps in the time series. The total time period has been split into two parts of 100 weeks duration. An autospectrum has been computed on each of these samples and then, the two available autospectra have been averaged to obtain the final autospectrum for SSH.

[15] The resolution of the autospectra was increased by adding zeros on either side of the temporal and spatial series (technique of zero padding). The energy at a specific spatial and temporal frequency is given by the amplitude of the peak. The phase velocity can then be computed, along with a confidence interval.

#### 2.4.2. Cross and Coherence Spectra

[16] In a manner similar to what was done for the autospectra of sea-surface chlorophyll, cross spectra have been computed between SSH and sea-surface chlorophyll. The peaks in the cross spectra identify the time frequencies and the wave numbers at which two signals correlate best, as well as their phase relationship. From the autospectra and the cross spectrum, the coherence spectrum can be computed by dividing the latter by the squared root of the former. Coherence is an indicator of the existence of a linear and stationary relationship between two signals. For both autospectra and cross spectra, a local maximum appeared clearly

at all latitudes. The frequency and wave number associated with these peaks were determined by averaging the eight pixels surrounding the maximum value using weights corresponding to the amplitude values (see Figure 4 in section 3).

## 2.5. Conceptual Rossby Wave Model From Killworth *et al.* [2004]

[17] To infer which Rossby wave-related physical and/or biological processes generate a chlorophyll signature, Killworth *et al.* [2004] designed a simple conceptual model which predicts ratios of the sea-surface chlorophyll to SSH anomalies. In this model, chlorophyll concentration ( $C$ ) and sea surface elevation ( $\eta$ ) are decomposed into the sum of a mean background level and a perturbation caused by the Rossby wave,

$$C = \bar{C} + C_A \text{ and } \eta = \bar{\eta} + \eta_A$$

where  $\bar{C}$  is the mean chlorophyll concentration,  $C_A$  the chlorophyll anomaly,  $\bar{\eta}$  is the mean sea-surface elevation,  $\eta_A$  the sea height anomaly.

[18] Assuming several approximations detailed in Appendix A, Killworth *et al.* [2004] derived a simplified equation to determine the theoretical ratio of generated  $C_A$  to  $\eta_A$  related to the wave

$$\frac{C_A}{\eta_A} = \frac{g}{f} \frac{(\bar{C}_{0y} - \beta C_z / f)}{(c - \bar{u}_0 + ic / \omega \tau)}$$

[19] The  $x$ ,  $y$ ,  $z$  axes are oriented eastward, northward and upward, respectively. Here  $g$  denotes gravity,  $F$  the Coriolis parameter,  $\beta$  the meridional gradient of the Coriolis parameter,  $C_{0y}$  the meridional gradient of chlorophyll,  $C_z$  the difference between  $C$  ( $z = 0\text{m}$ ) and  $C$  ( $z = 50\text{m}$ ),  $c$  the wave speed,  $u_0$  the zonal mean flow,  $w$  the wave frequency. Here  $\tau$  represents a relaxation time for a total nutrient anomaly to return toward zero by either physical (mixing) and/or biogeochemical processes (local consumption by phytoplankton). In the work by Killworth *et al.* [2004], the value of this parameter was determined from observations and set to 20 days. The phase lag between SSH and sea-surface chlorophyll is given by the argument of the ratio  $\frac{C_A}{\eta_A}$

[20] The ratio  $\frac{C_{0y}}{\beta C_z / f}$  represents the ratio of meridional horizontal to vertical advection (see Appendix A). The phase depends on the balance between zonal mean flow  $u_0$  and  $\omega \tau$ . For the case of a physical mechanism causing perturbations (or anomalies) in chlorophyll concentration, the respective contributions of horizontal and vertical advection to the chlorophyll anomaly can be calculated. The biological hypothesis will also be addressed in the discussion.

[21] Apart from the angular frequency  $\omega$  and wave speed  $c$ , which are deduced from the observations, the other model parameter values are selected as follows:

[22] 1. The meridional gradient in chlorophyll ( $C_{0y}$ ) is computed from the SeaWiFS data. Its zonal variations are quite strong whereas its alongshore variations, although rather noisy, are weaker (Figure 2). At the scale of the Peru region, we simplified the problem by considering  $C_{0y}$  as a function of the distance to the coastline. The variation of  $C_{0y}$  with distance to the coastline is approximated with a

linear function which decreases from  $10^{-5} \text{ mg m}^{-4}$  at a distance of 2 degrees from the coast, to a minimum value of  $10^{-6} \text{ mg m}^{-4}$  at a distance of 5 degrees from the coast.

[23] 2. The surface zonal mean flow  $u_0$  is  $10 \text{ cm/s}$  in this region [Strub *et al.*, 1998]  $\tau$  is set to 12 days. This value was obtained from a global ocean modeling study on artificial iron fertilization using an ecosystem model [Aumont and Bopp, 2006]. As shown in the latter study, this value is in good agreement with the results of IRON-EXII [Coale *et al.*, 1996].

[24]  $C_z$  was computed from chlorophyll data obtained from IMARPE (J. Ledesma, personal communication, 2005). In situ chlorophyll data are available at the sea-surface, 10, 25 and 50 m.  $C_z$  is considered constant zonally between  $2^\circ$  and  $8^\circ$  from the coast. The mixed layer is 15 m depth in summer and about 60 m depth in winter at this distance from the coast. We chose  $C_z = C_{\text{surface}} - C_{25\text{m}}$ , as the average depth of the mixed layer is around 25m, in the region [de Boyer-Montégut *et al.*, 2004]. Note that chlorophyll concentration variations are likely to be minor between 25 and 50 meters depth when the mixed layer is shallow, i.e., during spring and summer, the time period during which the Rossby waves influence on sea-surface chlorophyll concentration is observed. Data from summer cruises between January and March of the years 1998–2004 were averaged.  $C_z$  was calculated at a distance of 300 km from the coast at four latitudes:  $5^\circ\text{S}$ :  $-0.3 \text{ mg/m}^3$ ,  $6^\circ\text{S}$ :  $-0.57 \text{ mg/m}^3$ ,  $9^\circ\text{S}$ :  $-0.85 \text{ mg/m}^3$ , and  $12^\circ\text{S}$ :  $-0.33 \text{ mg/m}^3$ . These values were then interpolated linearly between  $5^\circ\text{S}$  and  $12^\circ\text{S}$  for model use.

[25] Having carefully chosen the values of the parameters, the Killworth *et al.* [2004] model was run in the following region: between  $2^\circ$  and  $8^\circ$  from the coast of Peru and between  $5^\circ\text{S}$  and  $12^\circ\text{S}$ , where propagations of the chlorophyll signal were most evident (Figure 3).

## 3. Results

[26] It can be seen in Figure 1 that variations in chlorophyll concentration have amplitudes of order 5–100% of the mean chlorophyll concentration. As the spatial characteristics of these fluctuations are present in the intraseasonal filtered signal, these fluctuations are not caused by the seasonal cycle (data not shown). As a first attempt to evaluate whether westward propagative patterns contribute to that variability, a time-longitude diagram of sea-surface chlorophyll at  $5^\circ\text{S}$  is shown in Figure 3b. Westward propagating events at intraseasonal periods between 2 and 4 months are clearly visible as diagonal stripes. They extend far from the coast between  $4^\circ\text{S}$  and  $9^\circ\text{S}$  (Figure 3b). They seem to determine the offshore limit of the highly productive region related to the upwelling. The occurrence of these intraseasonal events seem to be independent of the seasonal cycle. Nevertheless, their amplitudes may vary seasonally, as the coastal upwelling is more intense in austral winter. When intra-annual SSH anomalies and sea-surface chlorophyll propagation events are superimposed (Figure 3a), the two events seem well correlated. Furthermore, positive sea-surface chlorophyll anomalies slightly lead maximum positive anomalies in SSH.

[27] Propagation velocities were estimated by calculating the slopes of the rays on the time-longitude diagrams

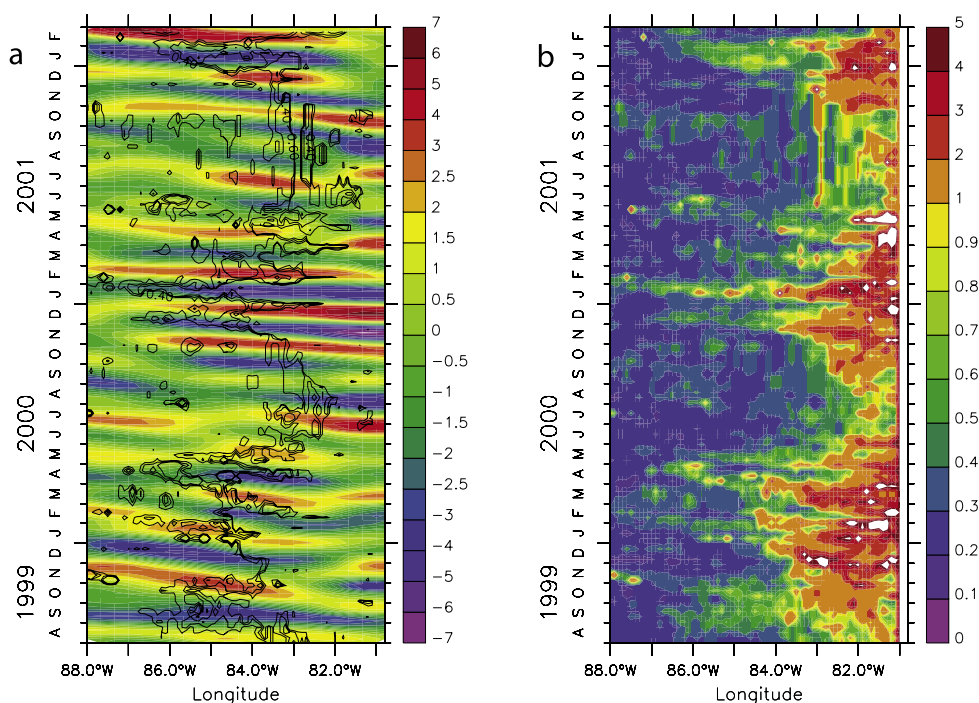


**Figure 3.** Time longitude plots along  $5^{\circ}\text{S}$  of (a) extracted intraseasonal Sea surface height (SSH) anomalies (in cm) from T/P-ERS. The black line displays the  $0.5\text{ mg Chl/m}^3$  isoline of surface chlorophyll (SCHL) concentration. (b) SCHL in  $\text{mg Chl/m}^3$ . The white shaded areas represent the cloudy periods.

(Figure 3b). This speed tends to be maximal in the area closest to the equator and to decrease poleward (not shown), consistent with the beta effect on Rossby waves speeds. Even if this estimate is quite imprecise and rather qualitative, the mean propagation speed is of order  $10\text{ cm/s}$ . The spatial and temporal resolution, the noise in the chlorophyll signal and the variability of the propagative events preclude a more accurate estimate of this value.

[28] After extraction of the intraseasonal westward propagating SSH, the autospectrum clearly reveals a dominant intraseasonal component at each latitude between  $5^{\circ}\text{S}$  and  $12^{\circ}\text{S}$  (see Figure 4 as an example for  $7^{\circ}\text{S}$ ). These peaks have associated temporal and spatial periods which vary from the north to the south of the region (Figures 5a–5c): The temporal period of the dominant wave is 60 days at  $5^{\circ}\text{S}$ , increases up to 120 days at  $9^{\circ}\text{S}$  and remains constant at approximately 80 days south of  $9^{\circ}\text{S}$ . The spatial wavelength associated to the peak in the autospectra decreases monotonically from 9 degrees ( $\sim 1000\text{ km}$ ) at  $5^{\circ}\text{S}$  to 4 degrees ( $\sim 450\text{ km}$ ) at  $9^{\circ}\text{S}$  and then increases to 6 degrees ( $\sim 650\text{ km}$ ) at  $12^{\circ}\text{S}$ . The phase speed of the wave, calculated as the ratio between the spatial wavelength and the temporal frequency, lies between 5 and  $25\text{ cm/s}$ . The speed is maximum at  $5^{\circ}\text{S}$  ( $\sim 20\text{ cm/s}$ ), decreases rapidly poleward, reaches a minimum at  $9^{\circ}\text{S}$  ( $5\text{ cm/s}$ ) and increases again slightly south of  $9^{\circ}\text{S}$  (Figure 5c).

[29] Secondary peaks clearly appeared at some latitudes. However, their amplitude was much weaker than the dominant peak. Furthermore, and perhaps more importantly, no systematic pattern or tendency could be deduced from their positions as their location seemed to vary rather randomly over the latitudinal domain. Moreover, these peaks were often at the limit of the resolved band in the

spatial and temporal frequencies space, and might have been artificially generated by the spectral analysis as the analyzed time series were rather short. This led us to focus on the most energetic peak in the autospectra and cross spectra.

[30] The SSH-chlorophyll cross spectra exhibit significant peaks in the studied latitude range (from  $5^{\circ}\text{S}$  to  $12^{\circ}\text{S}$ ), and the amplitude of these peaks decreases poleward (Figure 6a). This pattern is expected as the amplitude of filtered SSH anomalies decreases poleward whereas the amplitude of chlorophyll anomalies remains almost constant. When compared to the SSH autospectra (Figure 5), they show rather similar tendencies. However, the cross-spectrum analysis produces spikes, most noticeably at the lowest temporal frequencies which do not exist in the autospectrum analysis. We shall return to this point shortly.

[31] Figure 6b presents the coherence between the SSH and SCHL time series. The coherence is approximately 0.8 in the  $5^{\circ}\text{S}$ – $12^{\circ}\text{S}$  band (see Figure 6b). It decreases slightly poleward, and falls occasionally under the significance level threshold value (0.63 in the present case). Consequently, the correlation between the SSH and chlorophyll signal is more significant near the equator than poleward of  $9^{\circ}\text{S}$ . The argument of the coherence, which represents the phase shift between the sea-surface chlorophyll and SSH filtered signals, can be considered reliable between  $5^{\circ}\text{S}$  and  $9^{\circ}\text{S}$  and more uncertain between  $9^{\circ}\text{S}$  and  $12^{\circ}\text{S}$ . This phase shift between the two signals varies relatively smoothly with the latitude, and lies between  $\pi/2$  and  $2\pi/3$  (Figure 7). Its sign is in agreement with that of the phase shift calculated by Killworth *et al.* [2004] farther offshore of the Peru region [see Killworth *et al.*, 2004, Figure 6]. This means that the process of horizontal advection of chlorophyll by the Rossby wave currents controls the variability.

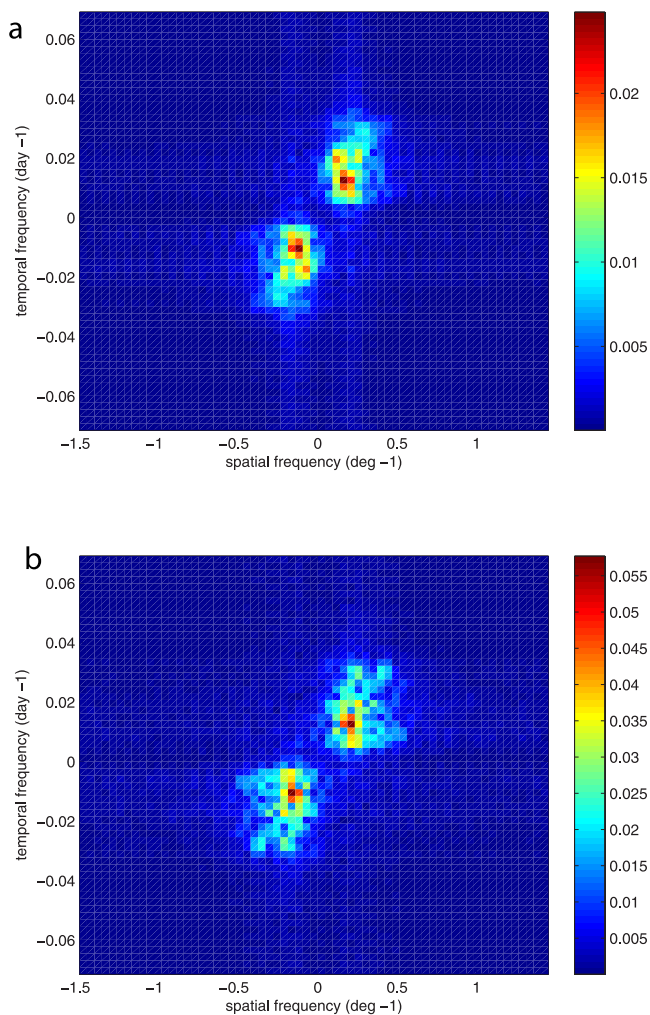


**Figure 4.** SSH autospectra and SSH-SCHL cross spectra at 7°S. (a) Autospectrum amplitude of filtered and normalized SSH signal in  $\text{day}^{-1} \text{deg}^{-1}$  (see section 2.4 for method). The 90% confidence interval for standard deviation is indicated on the right of the plot. (b) Cross-spectrum amplitude of filtered and normalized SCHL and SSH signal in  $\text{day}^{-1} \text{deg}^{-1}$ . The 90% confidence interval for standard deviation is indicated on the right of the figure. It represents the amplitude of the Fourier spectrum that can be considered as noise. Above this interval, a peak can be considered as significant.

[32] The amplitude of the intraseasonal sea-surface chlorophyll anomalies caused by the propagation of the Rossby waves can be computed by selecting the amplitude of the sea-surface chlorophyll autospectra at the wave number and frequency of the peak in the SSH–sea-surface chlorophyll cross spectra. Between 5°S and 12°S, the amplitude of sea-surface chlorophyll anomaly follows the same pattern from the north to the south (not shown). It varies between 15% and 25% of the averaged total chlorophyll concentration, depending on the distance to the coast: The percentage value is low close to the coast, reaches a maximum offshore and decreases farther away from the coast (same spatial structure as on Figure 1 and Figure 2, not shown).

[33] This result needs to be compared to typical fluctuations of chlorophyll concentrations around the mean total chlorophyll concentration. As noted previously, the standard deviation represents between 50% and 100% of the mean chlorophyll concentration (see Figure 1). It means that the amplitude of the signal induced by the Rossby waves can reach about 25% of the typical fluctuations observed in this region. The total variance of the chlorophyll concentration signal can be calculated by summing peaks on chlorophyll autospectrum (data not shown). If we compare with the variance included in the peak corresponding to intraseasonal frequencies, we calculate that chlorophyll fluctuations at these frequencies represent on average 10% of total chlorophyll variance. Moreover, the coherence spectrum SSH–sea-surface chlorophyll shows that in average Rossby waves explain 80% of chlorophyll variance at the peak of the cross spectrum. As a conclusion, it means that intraseasonal Rossby waves explain 80% of the 10% of total variance corresponding to the intraseasonal band, and hence 8% of total chlorophyll variance. This shows that Rossby waves have a strong signature in the Peru upwelling region, of the same order of magnitude as 10 to 20% of total variance obtained globally [Uz *et al.*, 2001].

[34] In order to determine which mechanisms are responsible for generating the chlorophyll signal, the conceptual model of Killworth *et al.* [2004] (see section 2 and Appendix A) was used to compare the predicted and observed ratios of SSH to sea-surface chlorophyll anomaly related to the intraseasonal Rossby waves, presented in Figures 8a–8d. Both modeled and observed ratios are of the same order of magnitude in the northern part of the domain (between 5°S and 7.5°S) (Figures 8a and 8b). South of 8°S, the modeled ratio is too high (Figure 8a). As expected, the chlorophyll anomaly is stronger close to the coast owing to the more intense meridional gradient of chlorophyll nearshore, and decreases strongly farther offshore. The effect of advection terms is dominant everywhere in the area even though the influence of vertical advection increases equatorward (Figure 8d).

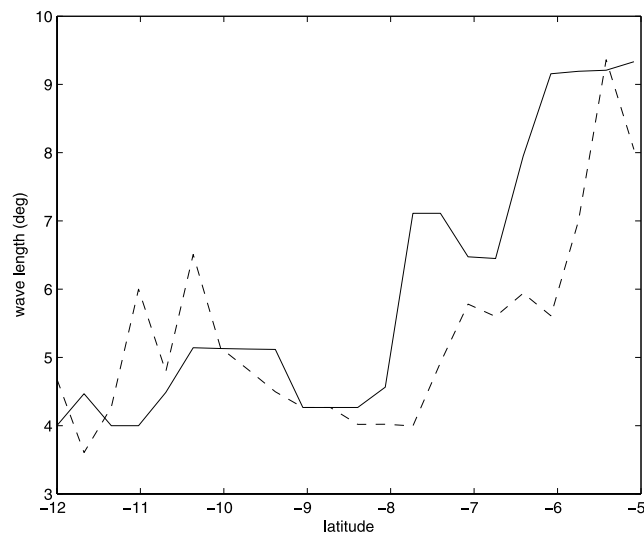


**Figure 5a.** SSH autospectra (solid line) and SSH-SCHL cross spectra (dashed line) variations versus latitude. Wavelength is given in degrees.

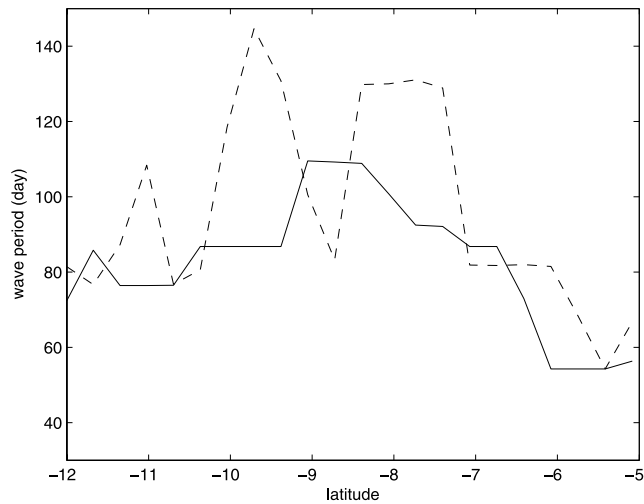


**Figure 5b.** SSH autospectra (solid line) and SSH-SCHL cross-spectra (dashed line) variations versus latitude. Wave period is given in days.

[35] The agreement between the model and the observations (Figure 8c) is better than in the work by *Killworth et al.* [2004], as their modeled ratio exceeded the observed ratio by a factor 10 at a distance of 5 degrees from the coast in the area of the eastern Pacific. The better agreement found in the present study likely stems from a better adjustment of the model parameters to the region of interest. However, south of  $8^{\circ}\text{S}$ , the chlorophyll anomaly decreases strongly and the model overestimates the observed ratio by a factor of  $\sim 5$ – $10$  (Figure 8c). Besides, the predicted and observed phase shifts are in close agreement between  $5^{\circ}\text{S}$  and  $10^{\circ}\text{S}$  (Figure 9). As the phase is determined by the balance between the terms in the denominator in equation (A1), this shows that the contribution of the mean zonal

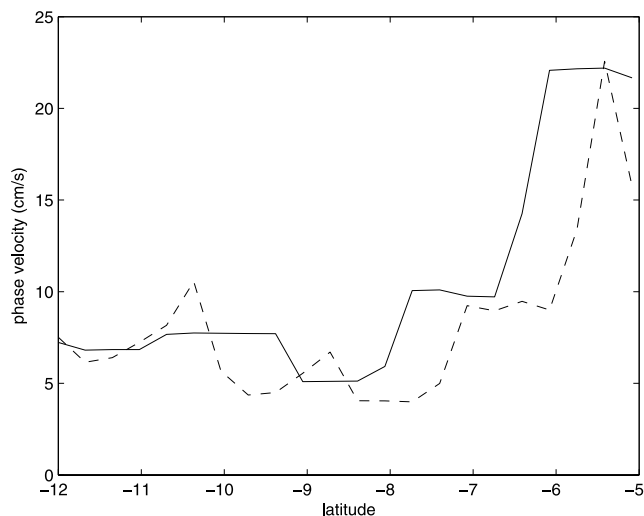


**Figure 5c.** SSH autospectra (solid line) and SSH-SCHL cross-spectra (dashed line) variations versus latitude. Phase speed is given in cm/s.

flow must be taken into account and that the value for the relaxation time  $\tau$  is accurate.

## 4. Discussion

### 4.1. Uncertainties

[36] The duration of cloudy periods in the vicinity of Peru was clearly limiting for this study. As we were careful not to perform indiscriminant interpolation of the ocean color signal, large gaps remained in the chlorophyll product. As a consequence, we had to work with shorter time series. Hence the temporal length of each continuous set of observations cannot exceed 30 weeks for sea-surface chlorophyll. Furthermore, focus was given to a region whose zonal extent is 20 degrees from the coast, meaning that spatial and temporal resolution for chlorophyll autospectra and SSH-chlorophyll cross spectra are 10 degrees spatially and 105 days temporally. The spatial resolution was not limiting as the spatial wavelength of the dominant signal never reached 10 degrees. However, such was not the case

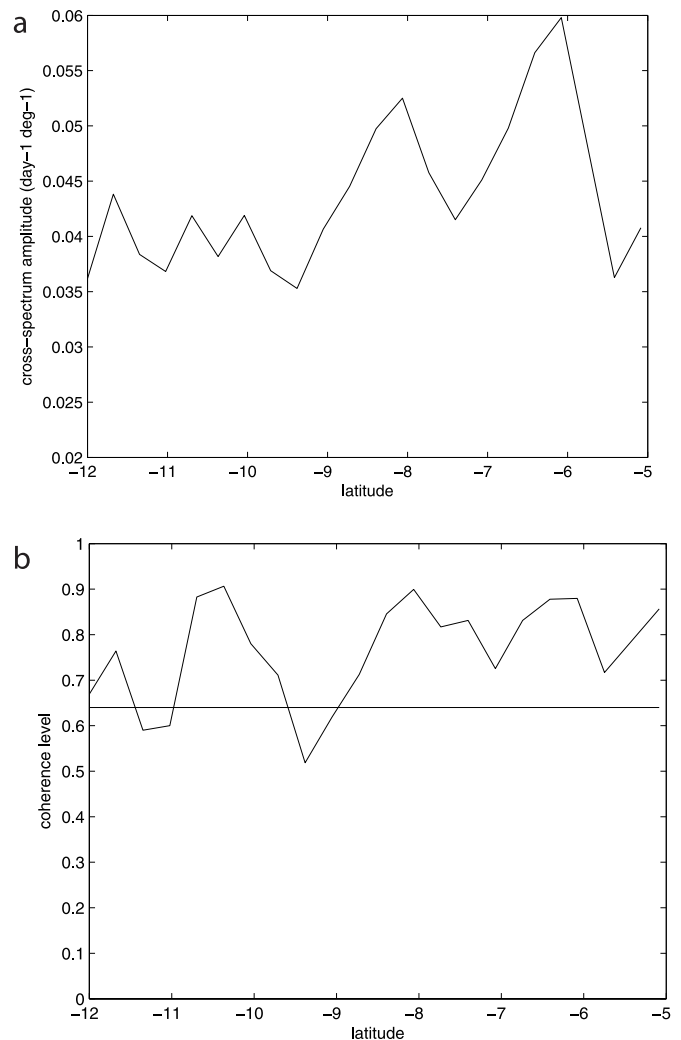


**Figure 6.** (a) Cross-spectral SSH-chlorophyll amplitude peak (in  $\text{deg}^{-1} \text{day}^{-1}$ ) and (b) coherence associated with the maximum amplitude of cross-spectrum SSH-chlorophyll versus latitude. The horizontal line indicates the threshold of significance level.

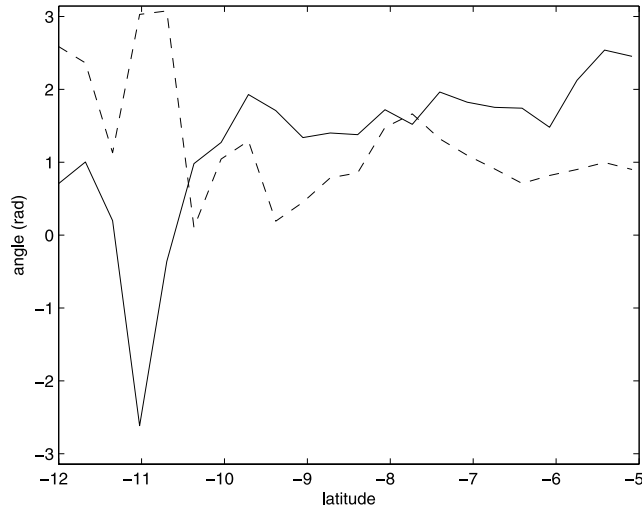


**Figure 7.** Phase shifts (in radians) between SCHL and SSH (full line) and between SSH and SST (dashed line) obtained from cross-spectral analysis versus latitude.

for the temporal resolution because some Rossby wave periods were close or slightly exceeded 105 days. As the SSH signal was not affected by cloudiness, the SSH autospectra were performed on a 100 weeks time series which allowed to detect Rossby waves periods up to 50 weeks long, i.e., 300 days. These considerations are important when SSH autospectra and SSH-chlorophyll cross spectra are compared (Figure 5). As noted previously, the temporal frequency of the dominant peak in the cross spectra displays significant fluctuations at values close to the temporal resolution of the spectrum (Figure 5a). However, a good agreement between the cross spectra and the SSH autospectra results can be observed for periods shorter than 100 days. Furthermore, the wave numbers are also consistent over the whole region (Figure 5b). These similarities suggest that the results deduced from the cross-spectral analysis are robust, even close the detection limit.

[37] The wave speed estimation is affected with uncertainties coming on the one hand, from the spatial and

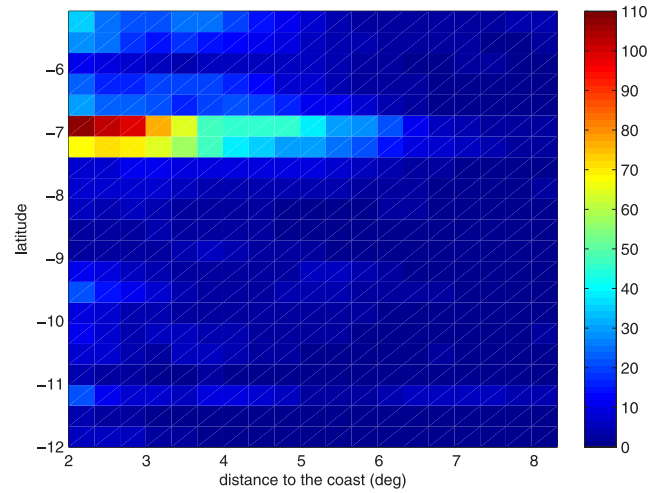


**Figure 8b.**  $C_A/\eta_A$  ratios from the observations.

temporal resolution of the satellite data, and on the other hand from the resolution of the 2D Fourier spectra. For the SSH autospectrum, we can estimate this uncertainty by adding the uncertainties coming from the spatial and temporal sources. With  $c$  denoting the Rossby wave phase speed calculated from the ratio of  $\lambda$  (wavelength) and  $T$  (wave period), we obtain the uncertainty  $\Delta c$ ,

$$\Delta c / c = \Delta \lambda_{\text{Topex}} / \lambda + \Delta \lambda_{\text{Spectrum}} / \lambda + \Delta T_{\text{Topex}} / T + \Delta T_{\text{Spectrum}} / T.$$

[38] If we consider the mean detected Rossby wavelength to be  $7^\circ$ , spatial uncertainty is the sum of the spectral uncertainty at this wavelength and of the uncertainty linked to the 7-day temporal resolution of the SSH product. Numerically, with  $c \sim 10$  cm/s being the mean phase velocity, the spatial uncertainty is equal to the sum of  $0.7/7$  (interval between 2 detected spatial periods on the spectrum for the  $7^\circ$  wavelength) and of  $0.5/7$  (the uncertainty on SSH data related to the wave propagation during 7days:  $10 \text{ cm/s} * 7 \text{ days} = 0.5$  degrees). The spatial uncertainty on phase speed is then  $\sim 17\%$ . Temporal uncertainty

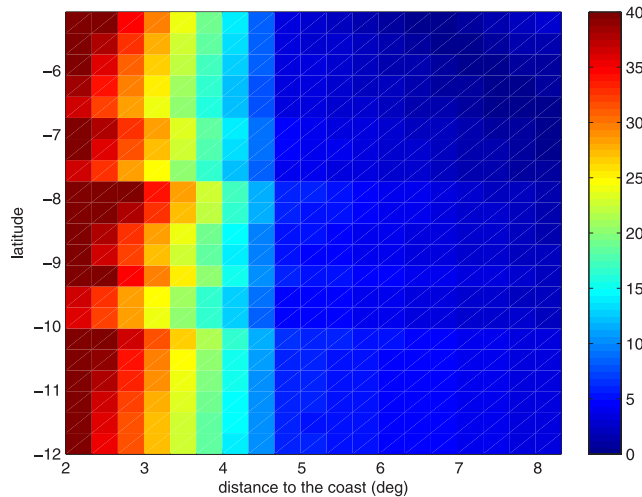


**Figure 8a.**  $C_A/\eta_A$  ratios from the model.

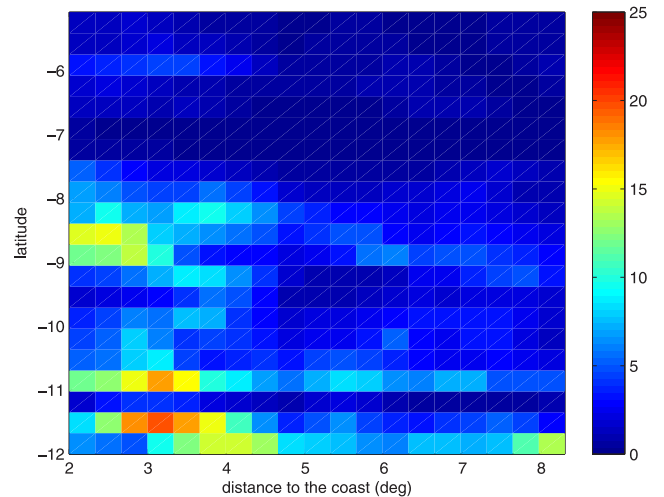


**Figure 8c.** Ratio of the modeled to observed  $C_A/\eta_A$ .

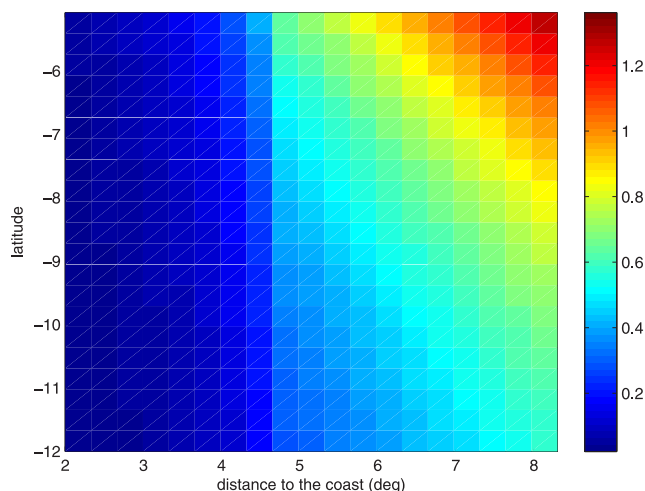


**Figure 8d.** Ratio of vertical advection to horizontal advection contribution.

around the 80 day time period is the sum of the spectral uncertainty (the resolution of the spectrum is 3 days for an 80 day time period) and of the uncertainty related to the temporal resolution of the composite (here 7 days). Temporal uncertainty is then equal to 13%. It follows that the total uncertainty on the calculated wave speed, for a wavelength of 7 degrees and a time period of 80 days, is approximately 30%.

[39] Additionally, a southward decrease of the cross-spectral amplitude peak and of the coherence was noted (Figure 6), meaning that chlorophyll and altimetry are less and less correlated poleward or that their amplitudes decrease. A possible explanation for this decrease could be an increase in cloudiness. Indeed, SeaWiFS data show more clouds in the southern part of the domain (not shown). Such higher cloudiness may result in a higher uncertainty on the chlorophyll signal. As the filtering procedure involves nearest neighbor filling of the gaps, the spatiotemporal components produced by the Fourier analysis could be noisier during winter. This was not the case with SSH since it is not affected by cloudiness. Such a differentiated impact could lead to a reduced correlation between SSH and SCHL, and to the generation of unexpected frequencies in the spectral analysis.

#### 4.2. Detection of Different Baroclinic Modes

[40] One particular result of Rossby wave related chlorophyll anomalies is the nonmonotonic variations with the latitude of the wave characteristics shown on Figure 5. Both time period and wavelength evolutions exceed uncertainties due to the method (see section 4.1) and are statistically significant. Consequently, the same nonmonotonic evolution is observed for the dominant wave speed. On the other hand, the presence of a single dominant Rossby wave mode would lead to a monotonic poleward decrease of the wave speed [Killworth *et al.*, 1997]. This pattern suggests that different Rossby wave modes may be dominating depending on the latitude range.

[41] Furthermore, the phase speed of the wave north of 9°S lies well below the expected value for a first mode

baroclinic wave at these latitudes. Indeed, phase speeds ranging between 5 cm/s and 22 cm/s for latitudes between 9°S and 5°S were computed from the spectra (Figure 5c). For a first baroclinic mode, theoretical phase speeds range from 30 cm/s and 70 cm/s [Killworth *et al.*, 1997]. Even if the 30% uncertainty inferred for these intraseasonal features is accounted for, the observed speeds remain much too low for a first mode.

[42] Let us now verify that local parameters, such as bottom topography changes or mean zonal flow variations, which could modify the phase speed, do not have a significant impact in the present case. When the effects of mean zonal flow and bottom topography changes are taken into account, the Rossby wave dispersion relation can be written as follows:

$$c = \frac{\omega}{k} = U - \frac{\bar{\beta}}{K^2 + L_D^{-2}},$$

with  $U$  the mean eastward flow,  $K$  the zonal wave number,  $L_D = gH/f_0^2$  the Rossby radius of deformation and  $\bar{\beta} = \beta + \frac{U}{L_D^2} + \frac{f_0 \Lambda}{D}$  with  $f_0$ , the local Coriolis parameter,  $\Lambda$  the eastward slope of the bottom,  $D$  the depth [Pedlosky, 1987]. Off Peru, the inner and outer shelves are significantly larger between 7°S and 10°S [Strub *et al.*, 1998], thus the eastward bottom slope is weakest in this latitude range. Therefore this topographic effect leads to a decrease of the theoretical wave speed between 7°S and 10°S according to the above equation. On the opposite, an increase in wave speed is observed, leading us to conclude that the topography cannot explain the observed variations. Besides, the mean zonal flow is supposed to be relatively constant with latitude between 5°S and 12°S [Strub *et al.*, 1998], whereas strong variations would be necessary to explain the observed variations of the speed and wave period around 8°S.

[43] These remarks suggest instead a change in the baroclinic structure of the dominant Rossby wave. Clarke and Shi [1991] predicted theoretically that poleward prop-

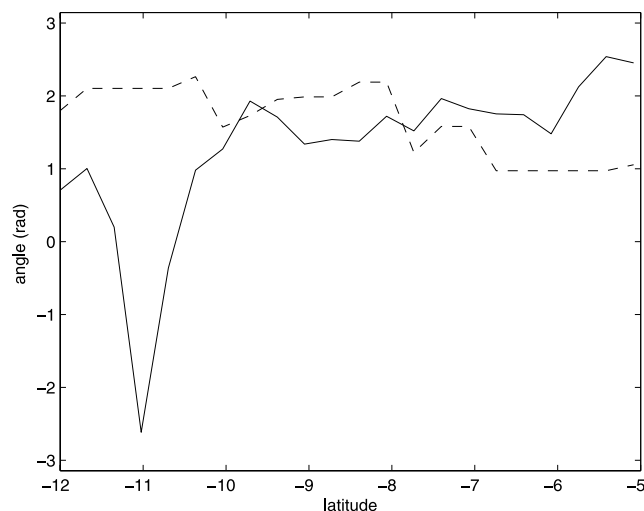


**Figure 9.** Modeled (dashed line) and observed (solid line) phase difference (in radians) between chlorophyll and SSH Rossby wave related signals. This phase, shown at 5° from the coast, varies very little with the longitude.

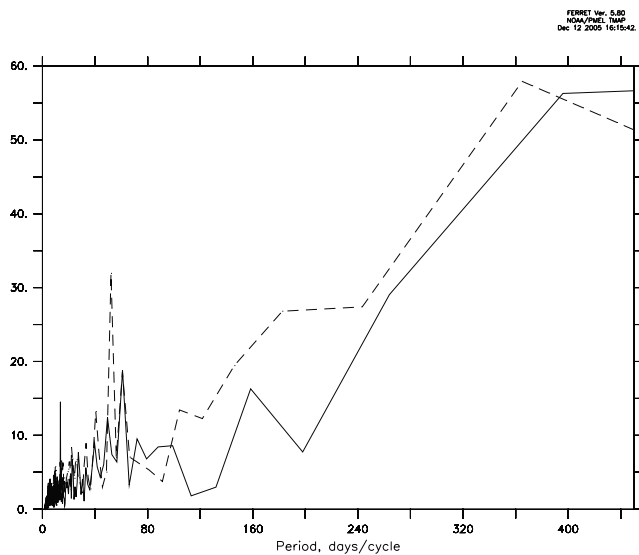


**Figure 10.** FFT spectrum of SSH from coastal tide gauges at Lobos ( $6^{\circ}\text{S}$ ) (solid line) and Callao ( $12^{\circ}\text{S}$ ) (dashed line).

agating Kelvin waves at a given time period can generate Rossby waves equatorward of a critical latitude, which depends on the time period and on the vertical structure of the Kelvin wave. Poleward of this latitude, the energy remains coastally trapped. According to this theory, a Kelvin wave with a second baroclinic mode vertical structure would generate a second mode Rossby wave everywhere between the equator and  $9^{\circ}\text{S}$  when the period exceeds 120 days. Similarly, a first mode Kelvin wave at 120 days would generate a first mode Rossby wave north of  $15^{\circ}\text{S}$ . The latitude  $9^{\circ}\text{S}$ , at which the wave characteristics change (Figure 5), corresponds to the theoretical critical latitude for the second baroclinic mode at 120 days. South of this limit, only a first mode Rossby wave at 120 days can propagate offshore. Therefore the detection of a dominant second baroclinic mode north of  $9^{\circ}\text{S}$  and of a first mode south of  $9^{\circ}\text{S}$  seems a reliable hypothesis.

[44] This suggests that the nonmonotonic evolution of the observed wave speed is due to the transition between two areas, the northern area being dominated by the propagation of second mode baroclinic Rossby waves and the southern area by first-mode baroclinic Rossby waves. Moreover, the estimated propagation speeds to the north are in closer agreement with second mode Rossby wave speeds whereas to the south, they are in relatively good agreement with the speed of a first mode, although slightly underestimated compared to values found in the literature [Killworth *et al.*, 1997]. Between  $10^{\circ}\text{N}$  and  $10^{\circ}\text{S}$ , first mode baroclinic waves propagate 50% faster than the phase speed deduced from the linear theory, whereas outside of the tropical area, phase velocities are rather overestimated [Chelton and Schlax, 1996]. Hence the value of the observed propagation speed alone cannot be trusted to determine which baroclinic mode is observed, especially in the studied area which is near the tropics. In the present study, the detected time periods and their agreement with those deduced from the theory of Clarke and Shi [1991] seem reliable elements

which indicate a latitudinal change in the vertical structure of the observed Rossby waves modes.

[45] The analysis of tide gauges data at  $6^{\circ}\text{S}$  and  $12^{\circ}\text{S}$  shows a significant peak at 70 days (Figure 10), whereas no peak appears at 120 days. This result is in agreement with the observed Rossby waves periods at these two latitudes (Figure 5b). In this region, tide gauges give information on coastal Kelvin waves, which may well be of equatorial origin. The absence of energy in the coastal sea level signal with a 120-day periodicity near  $9^{\circ}\text{S}$  and the presence of energy in the Rossby wave signal, suggests that an extratropical forcing, as for example local wind stress, could be acting. Indeed, several model studies show that the intra-seasonal variability in the ocean interior for the North Pacific [Fu and Qiu, 2002] and South Pacific [Vega, 2003] is driven by both the wind stress curl and the influence of the coastal boundary, depending on the latitude. In our region of study, Quikscat wind stress curl at  $\sim 100$  km from the coast, between  $4^{\circ}\text{S}$  and  $7^{\circ}\text{S}$ , displays a strong signal with a 120-day periodicity (data not shown). This indicates that 120-day period Rossby waves could be forced off the Peru shore between  $4^{\circ}\text{S}$  and  $7^{\circ}\text{S}$ .

[46] If we consider the Rossby wave efficiency in generating chlorophyll anomalies, the amplitude of the chlorophyll response to Rossby wave with respect to a given SSH anomaly is higher north of  $7^{\circ}\text{S}$  than south of  $7^{\circ}\text{S}$  (see Figure 8b). This could be related to a difference in the response to different baroclinic Rossby wave modes, as suggested by Killworth *et al.* [2004]. Indeed, if phase velocity decreases for a higher-mode Rossby wave, the eddy structure related to the wave propagates slower for a second mode, and the meridional currents can distort the chlorophyll surface fields more efficiently.

## 5. Mechanisms by Which Rossby Waves Act on Chlorophyll

[47] The use of the simple model suggests that horizontal advection is most likely responsible for producing the chlorophyll signal. In order to illustrate this, Figure 11 shows the time evolution of a chlorophyll anomaly together with the geostrophic velocities computed from SSH. Currents formed on the crests and troughs of a Rossby wave are assumed to be geostrophic because the spatial scales of Rossby wave associated eddies are much larger than the local Rossby radius of deformation. Moreover, the four snapshots are taken during the summer period when wind events were relatively scarce and weak. During the 4 weeks covered by Figure 11; sea-surface circulation was dominated by the geostrophic component and not by the Ekman current (negligible and not represented). On 27 November 1999 and 4 December 1999, chlorophyll patches elongate from the coast at  $6^{\circ}\text{S}$  toward the offshore region and seem to follow the trajectories suggested by the Rossby wave geostrophic currents. On 11 and 18 December, the geostrophic currents transport chlorophyll toward the coast. Such events highlight the dominant role of horizontal advection. Furthermore, Figure 11 shows that chlorophyll does not accumulate in convergence zones, which are located west of the wave crest in the southern hemisphere, and propagate zonally, with a front approximately parallel to the coastline [Dandonneau *et al.*, 2003]. In our case the

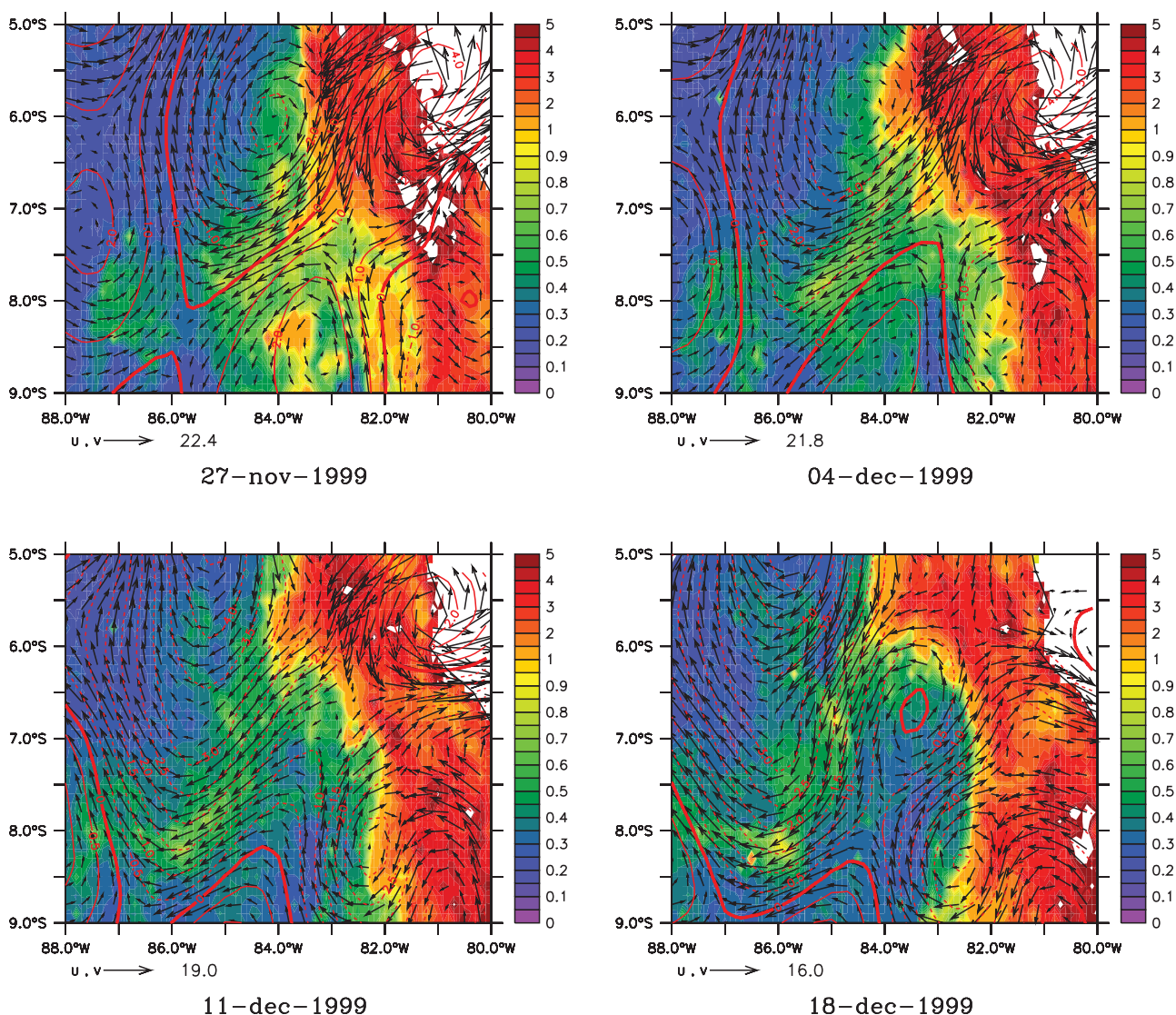


**Figure 11.** Chlorophyll patches detaching from the coast to the open ocean in summer 1997. Colors show the chlorophyll concentration (in  $\text{mg Chl/m}^3$ ). Red contours show the SSH anomaly (in centimeters). Black arrows indicate the geostrophic currents computed from the SSH anomalies. The time interval between each snapshot is 7 days.

elongation of the chlorophyll patch is approximately zonal and not meridional. Thus this is in disagreement with the “hay-rake” hypothesis, which specifies that the chlorophyll anomaly should be located in the convergence zone [Dandonneau *et al.*, 2003].

[48] The biological hypothesis proposes that the vertical advection of nutrients could be responsible for the propagating chlorophyll blooms [Killworth *et al.*, 2004]. This hypothesis also has to be rejected in the Peru upwelling region for two reasons. First, this hypothesis leads to a negative phase lag between chlorophyll sea-surface chlorophyll and SSH whereas a positive phase lag was found everywhere in the domain (Figure 7). Second, SST-SSH cross spectra show that the phase shift between SSH and SST is  $\pi/3$  (Figure 7). As a consequence, the phase shift between SST and sea-surface chlorophyll is equal to  $\pi$ . In other words, cold SST anomalies are in phase with positive chlorophyll anomalies. This observation does not allow us

to determine whether horizontal or vertical advection is dominant, because in both cases, high chlorophyll concentration would be collocated with cold waters. However, this result refutes the biological hypothesis once again. Indeed, as the phytoplankton bloom follows the injection of the nutrients in the euphotic layer, the phase shift between SST and chlorophyll should be less than  $\pi$ .

[49] Additionally, none of the terms in the first equation can be neglected a priori as they have the same order of magnitude, and thus may all play a significant role. In the northern part of the domain, vertical advection of chlorophyll represents up to 70% of the signal whereas it has a minor contribution in the south (see Figure 8d). Furthermore, the model produces rather satisfying results in the northern part of the region since the ratio ( $C_A/\eta_A$ ) and the SSH-chlorophyll phase shift compare well with the observations. This suggests that advection of chlorophyll itself is largely responsible for generating the chlorophyll anomaly.

Farther south, the observed ratio is overestimated by the model, especially south of 8°S. This discrepancy could be related to the change of Rossby wave vertical structure in evidence near 9°S. Further investigation would be necessary to better understand the impact of the vertical structure of Rossby wave on surface chlorophyll.

## 6. Conclusions

[50] This study underlines the impact of Rossby waves with periods around 90 days on the spatial and temporal variability of the highly productive Peru upwelling region. The influence of this dynamical process must be taken into account to understand the variability of offshore primary production at intraseasonal timescales. Copropagations of sea level and chlorophyll anomalies have been observed in the open ocean in previous studies. Their contribution to chlorophyll variability was estimated to about 10 to 20% on basin scale [Uz *et al.*, 2001]. In the Peru upwelling region, we show that Rossby waves may contribute to up to 8% of the chlorophyll variance, which is consistent with previous studies concerning the open sea whereas we are here situated in a coastal area. As only 8% of total sea-surface chlorophyll variability is explained by Rossby waves related transport, the influence of this process may seem relatively minor at first sight. However, this result has to be compared with the variance due to the seasonal cycle, which is equal to 82% of the total variance [Thomas *et al.*, 2001]. Thus Rossby waves propagation explain close to half of the remaining variance and thus has a major impact on the variability at the intraseasonal timescale. The shift of a dominant second baroclinic Rossby mode north of 9°S to a first baroclinic mode south of this latitude was identified and it was shown that this is consistent with theory. Using the simple process model of Killworth *et al.* [2004], the mechanisms by which Rossby waves impact biological activity were investigated. It is shown that the dominant process is horizontal advection which transports chlorophyll to the open ocean, away from the richest nearshore zone.

[51] This work has also identified uncertainty surrounding processes in the Peru upwelling region, and addressing this is beyond the scope of this paper: the identification of the dominant baroclinic modes of the Rossby waves, the respective contribution of horizontal and vertical advection of chlorophyll and nutrients, the mechanisms which generate Rossby waves in this region (coastal Kelvin waves, wind stress curl, bottom topography). In a next step, a coupled dynamical and biogeochemical model of this region could be of great help to address these questions. Eventually, this work could also be transposed to other eastern boundary upwelling systems to study the link between high productivity extent and Rossby waves propagation.

## Appendix A

[52] The SSH ( $\eta$ ), the velocity field ( $u$ ,  $v$ ,  $w$ ) and chlorophyll concentration ( $C$ ) are decomposed in a sum of mean background and a perturbation caused by the wave,

$$C = \bar{C} + C'; \eta = \bar{\eta} + \eta',$$

$$u = \bar{u} + u', v = \bar{v} + v', w = \bar{w} + w'.$$

[53]  $C'$  and  $\eta'$  are assumed to satisfy the wave equation

$$C' = C_A e^{i\varphi}, \varphi = kx - \omega t, \eta' = \eta_A e^{i\varphi}.$$

[54] Chlorophyll, considered as a passive tracer, satisfies the advection equation

$$\frac{DC}{Dt} = M \quad (\text{A1})$$

where  $D/Dt$  denotes the total derivative, and  $M$  represents a mixing term which includes all non conservative processes.

[55] Rossby waves are assumed to propagate westward and the  $x$ ,  $y$ ,  $z$  axes are oriented eastward, northward and upward, respectively. Here  $u$ ,  $v$ , and  $w$  are the associated velocity components.  $u'$  is equal to zero because  $l$ , the meridional wave number in the wave equation, is neglected. The mean meridional flow is assumed to be weak in comparison with work by Strub *et al.* [1998]. The wave scale is large in comparison with the Rossby deformation radius, so the thermal wind equation leads to

$$v_0 = \frac{g}{f} \eta'_x. \quad (\text{A2})$$

[56] With all previous approximations, equation (A1) becomes, to the first order,

$$.C'_t + \bar{u}C'_x + \sqrt{C}_y + w'\bar{C}_z = M \quad (\text{A3})$$

[57] To approximate  $w'$ , K04 use the vortex stretching equation

$$\beta v' = f w'_z. \quad (\text{A4})$$

[58] By integrating from the surface to the mixed layer depth, it follows:

$$w'(z = -h) = -\frac{\beta h}{f} v'_0. \quad (\text{A5})$$

[59] Then  $w'\bar{C}_z$  is approximated by  $-\frac{\beta}{f} v'_0 \Delta C$  where  $\Delta C$  is the chlorophyll concentration difference between the surface and the bottom of the mixed layer.

[60] Substituting all the terms in equation (A3), we finally obtain

$$C'_{0t} + \bar{u}C'_{0x} + v'_0 \bar{C}_{0y} - \frac{\beta}{f} v'_0 \Delta C = -\frac{C'_0}{\tau}, \quad (\text{A6})$$

where  $\tau$  is the relaxation time it takes for the perturbation of chlorophyll induced by the wave to return to 0.

[61] Using the wave expressions of  $C_A$  and  $\eta_A$ , equation (A6) becomes

$$-i\omega C_A + \bar{u}_0 i k C_A + \frac{i k g}{f} \eta_A C_{0y} - \frac{\beta}{f} \frac{i k g}{f} \eta_A \Delta C = -\frac{C_A}{\tau}. \quad (\text{A7})$$

[62] Replacing  $k = \omega/c$  in (A7) leads to the ratio of amplitudes in section 2.5,

$$\frac{C_A}{\eta_A} = \frac{g}{f} \frac{(\overline{C_{0y}} - \beta c_z / f)}{(c - \overline{u_0} + ic/\omega\tau)}.$$

[63] **Acknowledgments.** We thank C. Menkes, L. Bopp, P. Soler, and B. Dewitte for fruitful discussions on this study. This work was supported by the PROOF program OCEVAR and by the ATI “sistema de Humboldt” program.

## References

- Alheit, J., and P. Bernal (1993), Effects of physical and biological changes on the biomass yield of the Humboldt Current Ecosystem, in *Large Marine Ecosystems: Stress, Mitigation and Sustainability*, edited by K. Sherman, L. M. Alexander, and B. D. Gold, pp 55–68, Am. Assoc. Adv. of Sci., Washington D. C.
- Aumont, O., and L. Bopp (2006), Globalizing results from ocean in situ iron fertilization studies, *Global Biogeochem. Cycles*, *20*, GB2017, doi:10.1029/2005GB002591.
- Carr, M. E. (2002), Estimation of potential productivity in Eastern Boundary Currents using remote sensing, *Deep Sea Res., Part II*, *49*, 59–80.
- Carr, M. E., P. T. Strub, A. C. Thomas, and J. L. Blanco (2002), Evolution of 1996–1999 La Niña and El Niño conditions off the western coast of South America: A remote sensing perspective, *J. Geophys. Res.*, *107*(C12), 3236, doi:10.1029/2001JC001183.
- Chavez, F. P. (1995), A comparison of ship and satellite chlorophyll from California and Peru, *J. Geophys. Res.*, *100*(C12), 24,855–24,862.
- Chelton, D. B., and M. G. Schlax (1996), Global observations of oceanic Rossby waves, *Science*, *272*, 234–238.
- Cipollini, P., D. Cromwell, P. G. Challenor, and S. Raffaglio (2001), Rossby waves detected in global ocean colour data, *Geophys. Res. Lett.*, *28*, 323–326.
- Clarke, A. J., and C. Shi (1991), Critical frequencies at ocean boundaries, *J. Geophys. Res.*, *96*(C6), 10,731–10,738.
- Coale, K. H., et al. (1996), A massive phytoplankton bloom induced by an ecosystem-scale iron fertilization experiment in the equatorial Pacific Ocean, *Nature*, *383*, 495–501.
- Dandonneau, Y., A. Vega, H. Loisel, Y. Du Penhoat, and C. Menkes (2003), Oceanic Rossby waves acting as a “hay rake” for ecosystem floating by-products, *Science*, *302*, 1548–1551.
- de Boyer Montégut, C., G. Madec, A. S. Fischer, A. Lazar, and D. Ludicone (2004), Mixed layer depth over the global ocean: An examination of profile data and a profile-based climatology, *J. Geophys. Res.*, *109*, C12003, doi:10.1029/2004JC002378.
- Fu, L. L., and B. Qiu (2002), Low-frequency variability of the North Pacific Ocean: The roles of boundary and wind-driven baroclinic Rossby waves, *J. Geophys. Res.*, *107*(C12), 3220, doi:10.1029/2001JC001131.
- Kawamiya, M., and A. Oschlies (2001), Formation of basin-scale surface chlorophyll pattern by Rossby waves, *Geophys. Res. Lett.*, *28*, 4139–4142.
- Killworth, P. D., D. B. Chelton, and R. A. de Szoeke (1997), The speed of observed and theoretical long extratropical planetary waves, *J. Phys. Oceanogr.*, *27*, 1946–1966.
- Killworth, P. D., P. Cipollini, B. M. Uz, and J. R. Blundell (2004), Physical and biological mechanisms for planetary waves observed in satellite-derived chlorophyll, *J. Geophys. Res.*, *109*, C07002, doi:10.1029/2003JC001768.
- Le Traon, P. Y. (1991), Time scales of mesoscale variability and their relationship with space scales in the North Atlantic, *J. Mar. Res.*, *49*, 467–492.
- McGillicuddy, D. J., A. R. Robinson, D. A. Siegel, H. W. Jannasch, R. Johnson, T. D. Dickey, J. McNeil, A. F. Michaels, and A. H. Knap (1998), Influence of mesoscale eddies on new production in the Sargasso Sea, *Nature*, *394*, 263–266.
- O’Reilly, J. E., et al. (1998), Ocean color chlorophyll algorithms for SeaWiFS, *J. Geophys. Res.*, *103*, 24,937–24,953.
- Pedlosky, J. (1987), *Geophysical Fluid Dynamics*, 710 pp., Springer, New York.
- Siegel, D. A. (2001), The Rossby rototiller, *Nature*, *409*, 576–577.
- Strub, T., J. Mesias, V. Montecino, J. Rutllant, and S. Salinas (1998), Coastal ocean circulation off western South America: Coastal segment (6, E), in *The Sea*, vol. 11, edited by A. Robinson and K. Brink, pp. 273–313, John Wiley, Hoboken, N. J.
- Thomas, A. C., J. L. Blanco, M. E. Carr, P. T. Strub, and J. Osses (2001), Satellite-measured chlorophyll and temperature variability off northern Chile during the 1996–1998 La Niña and El Niño, *J. Geophys. Res.*, *106*(C1), 899–915.
- Uz, B. M., J. A. Yoder, and V. Osychny (2001), Pumping of nutrients to ocean surface waters by the action of propagating planetary waves, *Nature*, *409*, 597–600.
- Vega, A. (2003), Ondes de Rossby, niveau de la mer et couleur de l’eau dans le Pacifique Sud, Ph.D. thesis, Lab. D’Etudes en Geophys. et Oceanogr. Spatiales, CNES, Toulouse, France.
- C. Bonhomme and V. Echevin, Laboratoire d’Océanographie et de Climatologie: Expérimentation et Approches Numériques, IPSL, Tour 44-45, 4, place Jussieu, F-75282 Paris Cedex 05, France. (ceblod@lodyc.jussieu.fr; vech@lodyc.jussieu.fr)
- O. Aumont, Laboratoire d’Océanographie et de Climatologie: Expérimentation et Approches Numériques, IPSL, Centre IRD de Bretagne, BP 70, F-29280, Plouzané, France. (olivier.aumont@ird.fr)